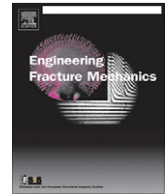




ELSEVIER

Contents lists available at SciVerse ScienceDirect

Engineering Fracture Mechanics

journal homepage: www.elsevier.com/locate/engfracmech

Crack initiation and path selection in brittle specimens: A novel experimental method and computations

O. Barkai^a, T. Menouillard^{b,1}, J.-H. Song^c, T. Belytschko^b, D. Sherman^{a,*}^a Department of Materials Engineering, Technion-Israel Institute of Technology, Haifa 32000, Israel^b Theoretical and Applied Mechanics, Northwestern University, Evanston, IL 60208-3111, USA^c Department of Civil and Environmental Engineering, University of South Carolina, Columbia, SC 2920, USA

ARTICLE INFO

Article history:

Received 17 July 2011

Received in revised form 13 March 2012

Accepted 8 April 2012

Keywords:

Experimental method

Mixed mode loading

Brittle isotropic materials

Crack path selection

Numerical calculation

ABSTRACT

We present a novel experimental method aiming at investigating aspects of dynamic crack propagation in brittle materials under in-plane, quasi-static, mixed mode loading. The method consists in gluing a precracked specimen into a rectangular hole in an aluminum frame using thin layers of epoxy resin. The driving force for crack initiation and propagation lies in the mismatch between the coefficients of thermal expansion (CTE) of the aluminum frame and the specimen, following modest heating of the assembly on an electrical heating stage. The main advantages of this method are in its avoidance of gripping problems and of the need to employ a complicated loading device. An important benefit of this method is the ability to analyze, numerically, the assembly containing the specimen as a boundary value problem by means of finite element analysis without any prior assumptions regarding the boundary conditions.

The method enables investigation of various aspects of dynamic crack propagation in brittle materials, including crack initiation, crack path selection criteria, and surface instabilities under a relatively low energy–speed regime. To validate the method's applicability, we first evaluated the fracture toughness, K_{IC} , of soda lime glass specimens. We then performed fracture experiments of slow and fast crack propagation in these specimens under combined tensile and shear stresses, which revealed the paths selected by the cracks. These paths were calculated using quasi-static finite element analysis (FEA), code Franc2D, and the dynamic eXtended FEA Method, using the criteria for crack path selection. It was found that the crack paths obeyed the law of local symmetry ($K_{II} = 0$) for both the quasi-static and dynamic crack propagation.

© 2012 Elsevier Ltd. All rights reserved.

1. Introduction

Brittle materials are currently gaining increasing attention due to their use as the main building blocks in high-tech industries, such as in the production of solar cells, Micro-Optical-Electro-Mechanical-Systems (MOEMSs), Nano-Electro-Mechanical-System (NEMS) industries, and in-bio inspired devices. The exact way in which cracks in brittle materials initiate and propagate is considered relevant not only from a scientific point of view, but also for design and maintenance purposes, which have considerable economic importance.

Investigating crack propagation in brittle specimens is challenging due to the need to generate controlled deformation of only a few tens of microns on the boundary of the specimen in order to initiate and propagate the crack. Such boundary

* Corresponding author.

E-mail address: dsherman@technion.ac.il (D. Sherman).¹ Present address: STUCKY SA, Rue du Lac 33, 1020 Renens VD 1, Switzerland.

conditions must be well defined if they are to be implemented as a boundary value problem for numerical analysis. Any deviations from the required deformation could lead to additional damaging mechanisms and energy dissipation that will be ignored or badly interpreted in the calculations, due to the high sensitivity of brittle materials to the fine details of loading.

The most challenging issue is that of how to grip brittle specimens while preventing undesired deformation and unexplained failure. Several methods for gripping and loading of brittle specimens when investigating crack propagation under quasi-static loading have been presented in the literature: fracture under bending [1,2], fracture of a compact specimen by introducing a wedge in a wide notch [3], mounting the specimen in a steel frame [4], and double cleavage drilled compression (DCDC) test method [5]. Thermal stress has been employed as the driving force for crack initiation and propagation, especially for MEMS devices [6].

The first objective of this study was to delineate and test a novel and simple method for gripping and loading precracked brittle specimens under mixed mode loading. The mismatch of the coefficients of thermal expansion (CTE) was exploited as the driving force for crack initiation and propagation. We fractured the soda lime glass specimens, representing a brittle and isotropic material, under both slow and intermediate crack speed regimes.

The second objective was to verify the ability of numerical methods and fracture laws to accurately predict the path selected by a crack in brittle isotropic materials subjected to quasi-static tensile and shear stresses. The theories that predict crack propagation are based on stress criteria or energy considerations: according to stress criteria, a crack will propagate so that the tensile stresses at the crack tip are either maximal or, alternatively, vanishing shear stresses [7]; while the energy criteria state that the crack will propagate so that the strain energy density is minimized, or the energy release rate is maximized [8]. The law of local symmetry states that a crack will propagate such that the shearing stress intensity factor (SIF) vanishes, i.e. $K_{II} = 0$ [9]. These laws have proven adequate for the prediction of slow cracks, such as fatigue cracks in metals, and static numerical simulations by the finite element analysis (FEA) have provided good predictions of the crack path obtained experimentally [10–12]. The ability to predict crack path selection for dynamic cracks under mixed mode loading with the appropriate criteria has also been shown [13–17].

We employed the quasi-static, linear elastic, and isotropic Franc2D FEA code, developed by Ingraffea and co-workers [10,12] to calculate the path selected by a slow crack, as this code is capable of efficiently analyzing quasi-static cracked bodies subjected to mixed mode loading with several crack path selection criteria under a single run. The eXtended FEA Method developed by Krysl and Belytschko [14] and Song et al. [18] was used to compute the path selected by a dynamic crack propagated in quasi-statically loaded specimens. This method allows the crack to propagate independently of the structure of the mesh, due to the use of enrichment functions, and thereby avoids re-meshing during propagation of the discontinuity [16,18–20]. The variant of the method used [18] is based on the technique of Hansbo and Hansbo [21]. The law of local symmetry, $K_{II} = 0$, was used for the simulations of the path selected by a fast crack with a cohesive law [18,22]. The numerical analyzes showed an excellent agreement with the experimentally-observed crack path.

2. The coefficients of thermal expansion mismatch (CTEM) method

2.1. The assembly

This novel experimental method consists of gluing a precracked rectangular and thin brittle specimen inside a rectangular hole in a 10 mm thick aluminum frame (Fig. 1a) using 150 μm thick layers of epoxy resin. Loading the specimen is achieved by applying controlled heating to the assembly on top of a heating stage. The mismatch between the coefficients of thermal expansion (CTE) of the aluminum and that of the brittle specimen generates tensile and shear deformation fields at the glued edges of the specimen, which serve as the driving force for crack initiation and propagation, as shown in Fig. 1b. The shear deformation field, like the tensile deformation, is generated by the mismatch of the CTE of the specimen and the loading frame in the x direction along the glued edges of the specimen: it is zero in the mid span ($x = 0$), and linearly increases towards the far edge points of the glued zone with opposite signs. This deformation is one of the unique advantages of our novel loading device: while being small compared to the tensile deformation, it generates sufficient mixed mode loading for investigating crack path selection in brittle materials.

We distinguish between two major types of precrack location that are responsible for two different modes: pure mode I is achieved when the precrack is located at the midline, i.e. $y = 0$ (point A in Fig. 1b); while in-plane mixed mode is achieved when the specimen is notched at $y > 0$ (point B, Fig. 1b), resulting in a curved crack path.

Atomistically-sharp precracks were introduced in the specimens by thermal shock. The specimens were first notched at the required position to a length of ~ 2 mm using a 150 μm thick diamond saw, followed by heating the specimens to 100–150 $^{\circ}\text{C}$ and then their immersion in a shallow water reservoir. This ensured stress singularity at the precrack tip. For those materials with relatively low fracture toughness, the assembly provides sufficient driving force for initiation and propagation of the crack still under the elastic regime of the epoxy glue, and without any damage at the interface between the epoxy glue and the other constituents of the assembly.

The aluminum frame was machined such that a gap of 300 μm was left for the two thin epoxy resin (Epon 815C) layers that glued the specimen. After gluing, the assembly was kept in a controlled temperature chamber at 23 ± 0.1 $^{\circ}\text{C}$ for four days for curing. After curing, the assembly was placed on a heating stage, and the temperature was increased at a moderate rate of about 0.5 $^{\circ}\text{C}/\text{min}$. This loading is slow enough to obtain an homogeneous temperature through the thickness of the glass

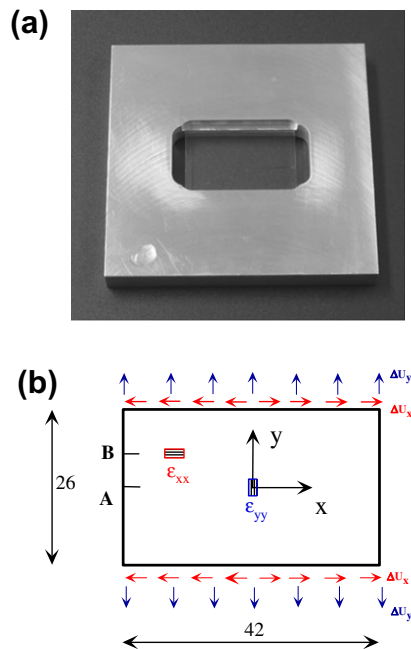


Fig. 1. The novel experimental set-up: (a) optical photograph of the frame and a glass specimen, and (b) schematic presentation of the specimen, boundary conditions, dimensions, and the location of the two typical precracks. The two strain gauges for the calibration procedure are also shown.

specimen and the aluminum frame. The maximum heating temperature is much below the glassy temperature of the epoxy resin. The Young's modulus of the epoxy resin is problematic to determine, as it strongly depends on the exact mixture of the two-part epoxy resin, curing time, and temperature. Since the stresses at the crack tip are dictated by this property, it was necessary to calibrate it by FEA based on measurements of the strains obtained by a strain gauge on each specimen during loading. The stress intensity factor at the crack tip at initiation and during propagation, $K_I(a)$, was calculated by means of FEA.

The specimens in the current investigation were made of commercially available 1 mm thick soda lime glass (Knittel Glaser, Braunschweig, Germany), with typical composition by weight as follows: 72–73% SiO_2 , 0.5–0.7% Al_2O_3 , 0.1–0.13% Fe_2O_3 , 12.7–13.1% $\text{Ca} + \text{MgO}$, 13.2–13.6% $\text{Na}_2\text{O} + \text{K}_2\text{O}$. The lateral dimensions of the specimen were $26 \times 42 \text{ mm}^2$.

2.2. Finite element analysis (FEA) of the assembly

We calibrated the assembly by FEA using Franc2D (Cornell University) [10]. The major obstacles in the analyses of our assembly were its 3D nature and the presence of the two thin ($\sim 150 \mu\text{m}$) epoxy resin layers. As the latter necessitate the use of small 3D elements, this would require massive analyses (in particular when multi-step calculations of crack propagation are required). Therefore, an equivalent 2D geometry was first defined that replicates the 3D nature of our assembly. This 2D geometry is shown in Fig. 2a. The material properties, the thicknesses, and the overall geometry in the 2D model are the same as those in the physical 3D assembly. Plane stress, linear elastic, quasi-static, and isotropic analyses were performed. The typical mesh describing our assembly, e.g., the specimen, epoxy resin layers, and loading frame, consisted in over 10,000 8-node isoparametric elements (Fig. 2b), of which 1500 were consisted the uncracked glass specimen. The details of the mesh at one corner of the assembly, including the thin epoxy glue layer, are shown in Fig. 2c. It is noted that Franc2D code automatically refines the mesh at the crack tip vicinity, refinement that is controlled by the user. This controlled refinement also provides the necessary information regarding convergence of the mesh, which was satisfactory achieved.

2.3. Experimental calibration

The properties of the aluminum plate were taken from the literature (see Table 1). The CTE of the epoxy glue is $26 \times 10^{-6} \text{ }^\circ\text{C}^{-1}$. The room temperature CTE of the soda lime glass, specified by the manufacturer, is $9 \times 10^{-6} \text{ }^\circ\text{C}^{-1}$ for the range of 50–350 $^\circ\text{C}$, while our measurements showed that it is $7.8 \times 10^{-6} \text{ }^\circ\text{C}^{-1}$ in the range of 20–30 $^\circ\text{C}$. This value, however, was not used in the FEA from two reasons: (i) during heating up of the assembly, the temperature of the aluminum loading frame is higher than that of the glass specimen and (ii) Franc2D allows to use a single unified ΔT for the entire problem.

The calibration process consisted of two $0.6 \times 0.6 \text{ mm}^2$ CEA-00-062UW-350 Vishay Ltd., strain gauges that were glued to an uncracked specimen: one at point (0; 0) that measures ϵ_{yy} ; and the other at point (–12.5; 7.7) that measures ϵ_{xx} , as schematically shown in Fig. 1b. The temperature in these experiments ranged from 22 $^\circ\text{C}$ to 29 $^\circ\text{C}$, which covers the entire

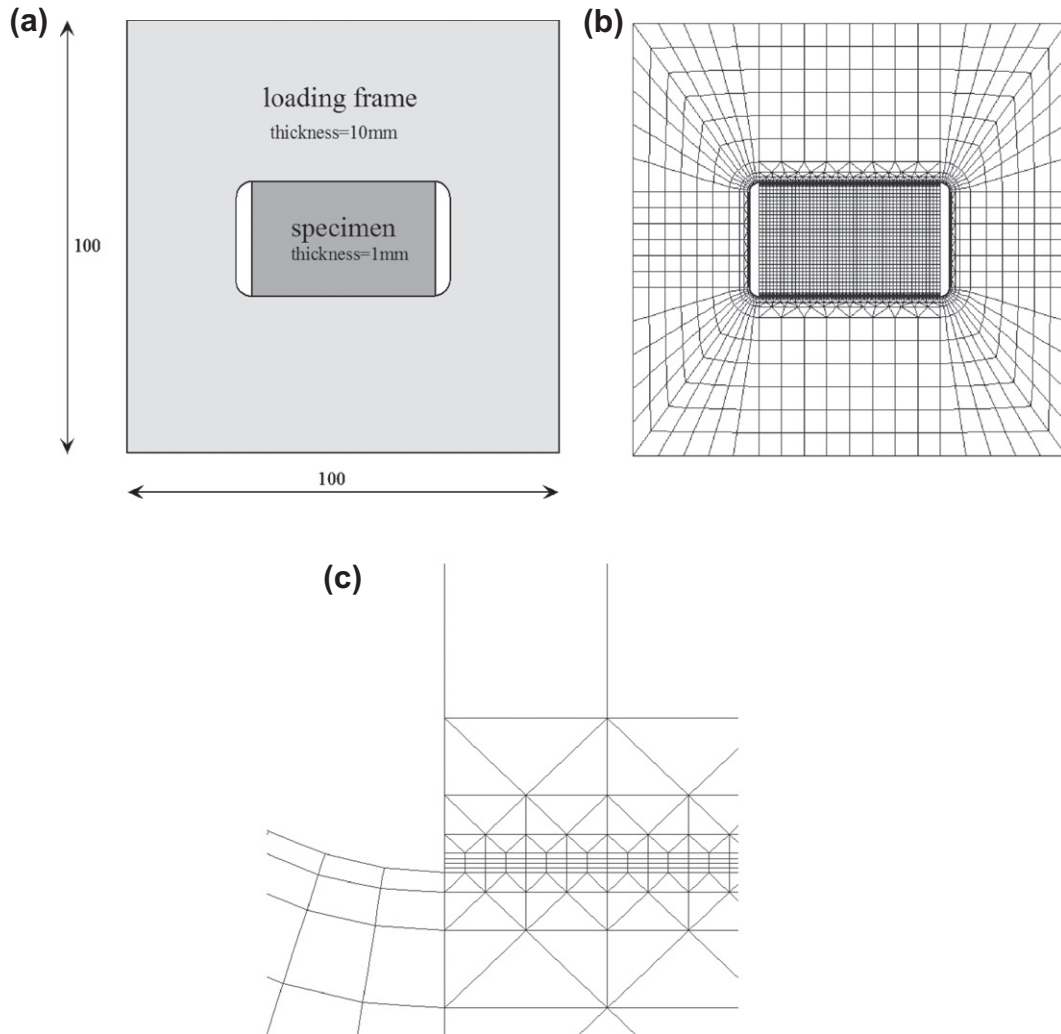


Fig. 2. The loading system as a 2D problem: (a) the equivalent 2D geometry substituting the 3D assembly, (b) the finite element mesh used by Franc2D code, and (c) details of the zone containing the frame, the specimen and the epoxy.

Table 1

The materials involved and their mechanical and thermal properties.

Material/properties	E (GPa)	ν	Thickness (mm)	α ($10^{-6} \text{ } ^\circ\text{C}^{-1}$)	ρ (kg/m^3)	k (W/m/K)	c_v (J/kg/K)
Al 7075-T6	75	0.33	10	26	2850	238	860
Soda-lime glass	73	0.22	1	7.8 (3 ^a)	2440	0.8	837
Epon 815C	2.1	0.3	0.15	26	1130		

^a This value was used to compensate the difference between the temperature of the loading frame during the experiment and that in the FEA.

range of the thermal differences in our fracture experiments. Heating the specimen to the temperature range was carried out in a slow and controlled manner by placing the assembly on top of a massive copper block that was inserted into a slowly heated water reservoir. In this way, a slow and stable temperature change was achieved during the strain measurements. The temperatures of the specimen and the loading frame were measured by means of two thermocouples.

It was first necessary to calibrate the response to temperature changes of the strain gauge glued to the glass specimen without mechanical loading, since its strain is of the same order of magnitude as the strain of the loaded specimen. The CTE of the soda lime glass at room temperature, as stated above, is $\sim 7.8 \times 10^{-6} \text{ } ^\circ\text{C}^{-1}$, while that of the strain gauge material (copper) is $23 \times 10^{-6} \text{ } ^\circ\text{C}^{-1}$. Consequently, negative strains were measured within the examined temperature range, which is usually ignored when large strains are measured, which was not the case in our experiments. This is well demonstrated in Fig. 3 for both ε_{yy} and ε_{xx} . After this calibration, the specimen with the strain gauge was glued to the aluminum loading frame and thermal loading was applied by heating the assembly. The resulting strains are also shown in Fig. 3.

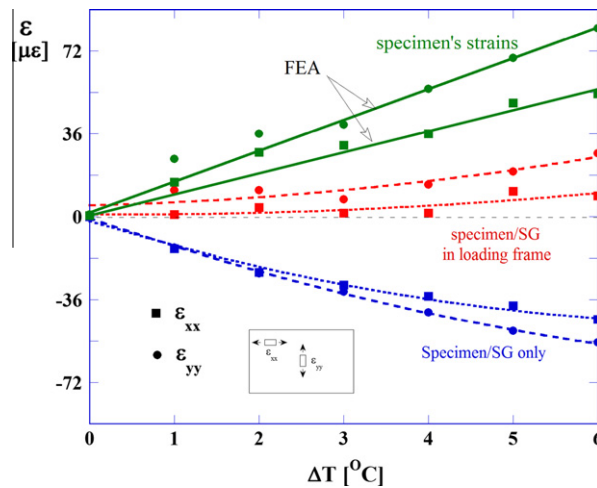


Fig. 3. The results of the calibration procedure: the strains measured by the strain gauges as a function of ΔT . The strains ε_{yy} (closed circles), located at $(0; 0)$, and ε_{xx} (closed squares), located at $(-6; 10)$, were measured both when the specimen with the glued strain gauge was free of constraint, and when it was mounted in the frame. The dotted lines represent curve fitting of the described strains. The solid lines describe the strains obtained by FEA using the materials' properties given in Table 1.

We set the CTE of the soda lime glass specimen to be $3 \times 10^{-6} \text{ } ^\circ\text{C}^{-1}$, as this value compensates the inability of the FEA code to match the exact temperature of the aluminum frame resulted with reduced deformation of the loading frame. By reducing the CTE of the glass specimen, we reduced the equivalent deformation of the specimen. Hence, we generated the same deformation on the epoxy resin layer, and therefore applied the same forces on the specimen. In addition, the Young's modulus of the epoxy glue was set to be 2.1 GPa.

Superposition of the strains in the free glass specimen and that of the specimen within the loading frame, using the reduced CTE and the elastic modulus of the epoxy resin yielded the mechanical strains in the glass specimen generated by the thermal stresses only (Fig. 3). Note the linear behavior of the experimental strains at $\Delta T \geq 3 \text{ } ^\circ\text{C}$. In addition, excellent agreement was achieved using these properties between the experimental and numerical crack path selection results (see below). The agreement between the experimental and the numerical values of the strains validates the calibration procedure, and indicates that the epoxy glue remained in the linear elastic regime during heating of the assembly in the temperature range of our experiments.

The contour levels of the quasi-static stress fields for the uncracked specimen, calculated by Franc2D, of σ_{yy} , σ_{xx} and σ_{xy} , assuming the epoxy resin Young's modulus is 2 GPa, are shown in Fig. 4a, b and c, respectively, for $\Delta T = 5 \text{ } ^\circ\text{C}$. Note the anti-symmetric double saddle behavior of the shear stresses: they are zero at lines $x = 0$ and $y = 0$ and increase in magnitude along the glued edges of the specimen. The former σ_{yy} stresses are responsible for the tensile (K_I) mode, and the latter σ_{xy} stresses for the shear (K_{II}) mode, provided that the crack tip is located off axis. The complex behavior of the shear stress in cracked specimens generated a complex ratio of K_{II}/K_I at the crack tip before initiation. This ratio is strongly dependent on the crack tip location and the angle of the precrack.

3. Calculating K_{IC} of soda lime glass

The SIF in tension, K_I , vs. crack length, a , along line $y = 0$ (type A crack, Fig. 1c), was first calculated as a prerequisite for evaluation of K_{IC} , the material property that is crucial for dynamic analysis of fast cracks. The $K_I(a)$ calibration function was first calculated by the J -Integral method using Franc2D with the mesh shown in Fig. 2b. The results are shown in Fig. 5. K_I monotonically increases as the crack length increases in a nearly bilinear shape. For up to 9 mm long precracks, K_I is low and increasing temperature differences, ΔT , are required in order to fracture the specimen. It is noted that the presence of the thin epoxy resin layers at the specimen's edges generated load-controlled condition for crack propagation, but the rate of increase of K_I was low for specimens containing long precracks in particular.

The fracture toughness of the soda lime glass was evaluated by measuring the precrack length and the temperature at crack initiation and by using the $K_I(a)$ relationship (Fig. 5). Experiments with two different precrack lengths of the A type crack (Fig. 1b) were performed at room relative humidity of $\sim 50\%$: in the specimen with a precrack of 6.5 mm, initiation was observed at $\Delta T = 5.5 \pm 0.1 \text{ } ^\circ\text{C}$; and in the specimen with a precrack of 10.5 mm, initiation was observed at $\Delta T = 4 \pm 0.1 \text{ } ^\circ\text{C}$. K_{IC} was evaluated to be 0.47 ± 0.04 and $0.49 \pm 0.06 \text{ MPa}\sqrt{\text{m}}$, respectively. While this value of K_{IC} is low compared to the data found in the literature for soda lime glass, it was shown recently [23] that K_{IC} of this glass, evaluated by Vickers indentation toughness technique and calculated by crack opening displacement using AFM scans, is $0.48 \text{ MPa}\sqrt{\text{m}}$ which is in excellent agreement with our results.

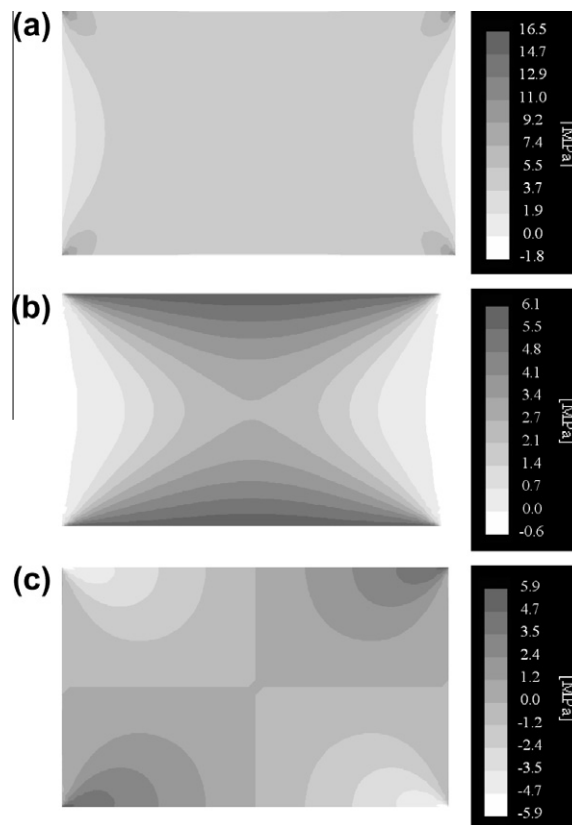


Fig. 4. The calculated contour levels of stress fields: (a) σ_{yy} , (b) σ_{xxx} and (c) σ_{xy} in an unnotched specimen. Note the even distribution and the dominance of σ_{yy} over σ_{xxx} and σ_{xy} .

4. Calculating crack paths

4.1. Analysis of slow crack propagation

When a long precrack is introduced into a specimen, only a small increase of K_I occurs during propagation, the excessive kinetic energy is relatively small, and the crack is expected to propagate at a low speed. Indeed, we describe here the path selected by a slow crack in a soda lime glass specimen. The specimen was precracked along line $y = 5.9$ mm above the center line (type B crack, see Fig. 1b), to a length of 16 mm. The crack initiated at 26 ± 0.1 °C and propagated at a velocity of a few mm/s for the first 10 mm. Thereafter, the crack accelerated to a somewhat higher speed until complete fracture. Optical photograph of the fractured specimen is shown in Fig. 6a. Both sides of the specimen were replicated using a high density scanner to obtain the path numerically.

The linear elastic and quasi-static analysis of the crack path was performed using Franc2D [10,12], as this code is able to calculate crack path selection under mixed mode conditions of isotropic materials using various criteria in an accurate and time-effective manner. Franc2D utilizes three different crack path selection criteria: maximum tensile stresses at the crack tip ($\sigma_{\theta\theta}$ max), maximum energy release rate ($G(\theta)$ max), and minimum strain energy density ($S(\theta)$ min). Rice J -Integral was used, by separating the tensile and shear elastic fields which yielding J_I and J_{II} , to calculate K_I and K_{II} . The resulting path predicted by the analysis is shown in Fig. 6b. All three crack path selection criteria evaluated the same path. The natural precrack is neither exactly perpendicular nor a perfectly straight crack; a fact that, although not considered in the analysis, presumably affects the path, at least at the beginning of propagation. We therefore dictated the numerical crack path for the first 3 mm (see arrow in Fig. 6b). It was found that after 3 mm the effect of the nonideal precrack surface vanished. The experimental crack velocity at this stage was low, the kinetic energy and the associated effects vanished and, therefore, the numerical solution well matched the experimental crack path. At point 27: 10, the crack started to accelerate, thereby confirming the prediction. This is further supported by the evolution of K_I with the x -coordinate, shown in Fig. 6b for $\Delta T = 3$ °C; the crack initiated at $K_I = 0.48$ MPa m^{1/2} and, until it had propagated for about 11 mm, K_I remained nearly constant, with no additional kinetic energy being generated. As the crack continued to propagate, K_I increased, the kinetic energy became significant, and the quasi-static analysis could no longer predict the crack path. Crack path selection using the three criteria and smaller crack intervals yielded the same path.

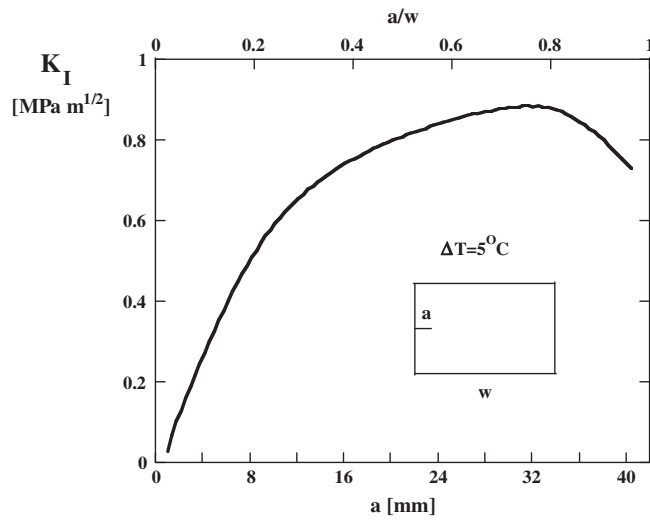


Fig. 5. The SIF K_I as a function of the crack length, a , and the normalized crack length, a/w , of a single edge, type A crack (see Fig. 1c) for the assembly materials described in Table 1.

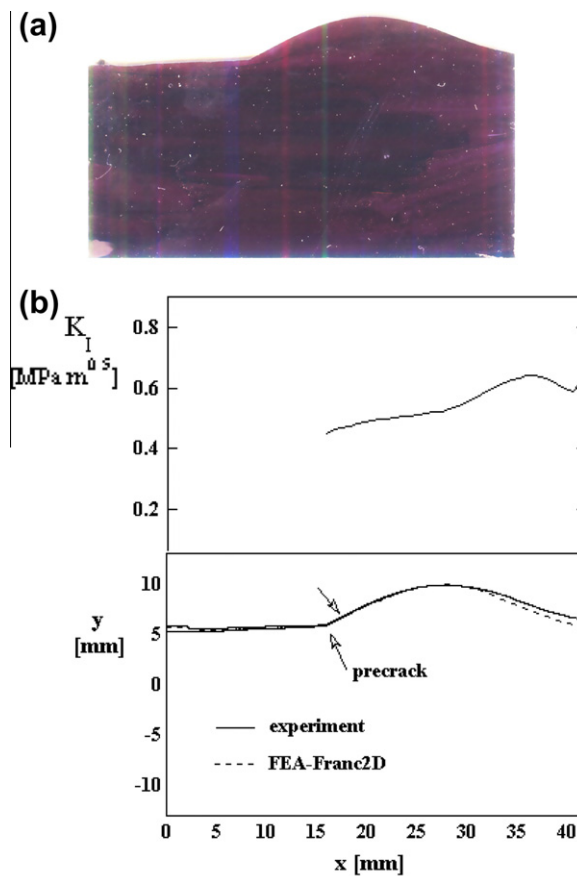


Fig. 6. The experimental and numerical crack path of a slow crack: (a) optical photograph of the fractured soda lime glass specimen, and (b) the experimental and numerical path (Franc2D) selected by a slow crack.

4.2. Analysis of fast crack propagation under mixed mode

The direction of crack propagation is determined by the law of local symmetry, i.e. $K_{II} = 0$ [9]. Nishioka and Stan [24] described this criterion as implicit, and its implementation was explained by Tilbrook and Hoffman [25,26]. The crack direction is first defined by the direction of the maximum hoop stresses. Thereafter, the direction for which $K_{II} = 0$ was calculated using iterative procedure. A method based on the formulation of the J -Integral was used to determine both K_I and K_{II} [28,29]. The glass specimen used for the dynamic analyses was modeled by 26×42 and 52×84 four-node element meshes, corresponds to a coarse and fine mesh [18,30]. The analyses were performed in two steps: first, the quasi-static thermal load was applied until the critical stress intensity factor was reached while the temperature increased from 23 °C to almost 28 °C. During the quasi-static simulation, the stress intensity factors, K_I and K_{II} , were computed (where $K_{II}/K_I < 0.15$ during crack propagation). Once K_I had reached the critical value, K_{Ic} , the dynamic simulation by the explicit method began with the final constant temperature. The temperature was chosen to be constant during the dynamic simulation as the temperature increase during crack propagation (which lasted $\sim 50 \mu\text{s}$) is negligible. This assumption is reasonable because the temperature increased by 0.5 °C per min.

A cohesive law was used on the crack faces. This law was fitted so that the energy dissipation matched that expected from the stress intensity factor of the material. The energy dissipated during the propagation, assuming plane stress state, was determined by:

$$G_f = \frac{K_{Ic}^2}{E} \quad (1)$$

where E is the Young modulus of the soda lime glass and K_{Ic} the critical stress intensity factor, evaluated in Section 4.1. This yielded $G_f = 3.16 \text{ Pa m}$, which was the value used to fit the cohesive law. The cohesive law was necessitated since energy dissipation mechanism other than bond breaking energy exists during crack propagation. Therefore a linear decay, as shown in Fig. 7, was used in the cohesive law, where the energy dissipated, Eq. (1), is given by:

$$G_f = \frac{1}{2} \delta_f \sigma_f \quad (2)$$

where δ_f is the maximum crack opening over which the cohesive law acts (Fig. 7) and σ_f is the fracture stress. These two parameters are determined during the computation by the fracture criterion. Their values are 0.003 mm and 2 MPa. The velocity V of the crack was prescribed using Freund equation of motion [27]:

$$V = C_R \left[1 - \left(\frac{K_{\theta\theta}}{K_{Ic}} \right)^2 \right] \quad \text{for } K_{\theta\theta} > K_{Ic} \quad (3)$$

where $C_R = 3200 \text{ m/s}$ is the Rayleigh free surface wave speed and $K_{\theta\theta}$ is the equivalent quasi-static stress intensity factor, defined by the dynamic stress intensity factors and the direction of the propagation θ_c :

$$K_{\theta\theta} = \cos^3 \left(\frac{\theta_c}{2} \right) K_I - \cos \left(\frac{\theta_c}{2} \right) \sin(\theta_c) K_{II} \quad (4)$$

The analyzed specimen contained a 6 mm long precrack, located at $y = 3 \text{ mm}$. The crack initiated at $28 \pm 0.1 \text{ °C}$. The short precrack caused sufficient kinetic energy to propagate dynamically. The fractured specimen showing the path selected by the dynamic crack is presented in Fig. 8a. The crack paths obtained by the experiment and by the numerical simulations with the two different meshes are shown in Fig. 8b. The law of local symmetry ($K_{II} = 0$) well matched the experimental path along the entire propagation, albeit with a certain deviation at the initial stage, presumably due to the imperfectly straight

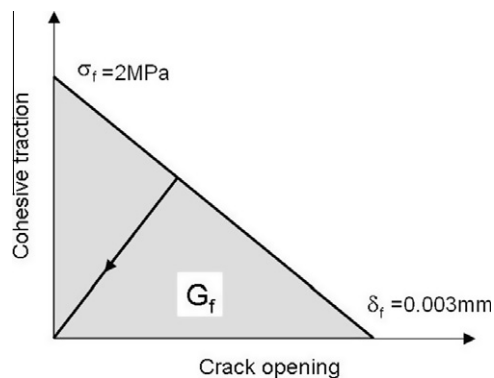


Fig. 7. Linear cohesive law; the area under the cohesive law curve is the same as the fracture energy G_f .

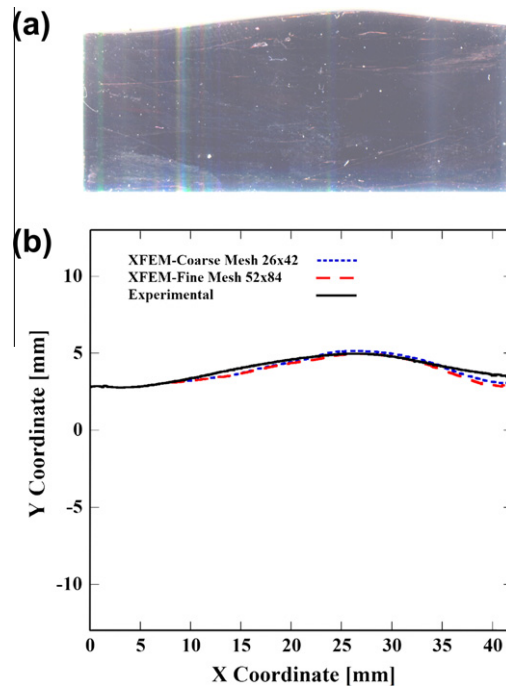


Fig. 8. Optical photograph of the fractured soda lime glass specimen revealing the crack path: (a) the short precrack ensured dynamic crack propagation with moderate crack velocity, and (b) the experimental (full black line) and numerical crack paths (red and blue dashed lines) in the specimen. The numerical paths (eXtended FEA Method) were obtained using coarse and fine meshes. (For interpretation of the references to colour in this figure legend, the reader is referred to the web version of this article.)

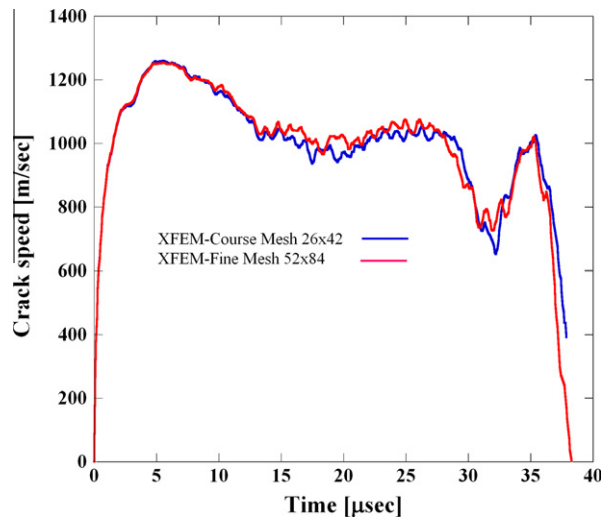


Fig. 9. Crack velocity as a function of time during fast crack propagation calculated by eXtended FEA Method using the coarse and fine meshes.

precrack. It started almost as a horizontal crack but then the shear stress field introduced an upward curvature. The predicted crack turned downward at almost the same point as in the experiment. The paths for the coarse and fine meshes agreed almost perfectly with the experimental results until the last quarter of the path. At that point, the computed path deviated slightly downward from the observed path. The agreement indicated that the boundary conditions in the numerical model closely matched those of the experiment. The results also substantiated the widely accepted law of local symmetry, $K_{II} = 0$, for dynamic crack propagation. The difference between the experimental and the numerical paths at the last stage of crack propagation may indicate on physical phenomenon, such as reflected stress wave from the far right boundary of the specimen. This behavior, however, is beyond the scope of this investigation.

The crack tip velocity as a function of time is shown in Fig. 9. Negligible difference between the prediction of the coarse and fine meshes is evident. The calculated maximum crack velocity is below 1250 m/s, which is below the onset of surface instabilities in soda lime glass [31]. This is consistent with the experimental findings of a mirror-like fracture surface. The steep crack velocity reduction at the end of crack propagation well fits the reduction of the quasi-static SIF at this zone, as shown in Fig. 5.

5. Summary and conclusions

We have presented here a novel experimental method by which to study crack initiation and propagation in a brittle material. The method exploits the mismatch between the coefficients of thermal expansion of the specimen and that of the aluminum loading frame in order to generate the driving force for crack initiation and propagation.

The fracture toughness of soda lime glass was evaluated in two fracture experiments; and the results, 0.47 and 0.49 MPa \sqrt{m} , are with excellent agreement with that obtained employing a more complicated procedure. The paths selected by a slow and a fast crack in soda lime glass were analyzed by numerical simulations. Quasi-static analysis, performed using Franc2D, was able to predict the experimental path selected by a slow crack for most of the crack path, using stress and energy criteria and the law of local symmetry. This analysis revealed that a deviation from the experimental path occurred when crack velocity reached a certain speed, which is not considered in the quasi-static FEA. The experimental fast crack was analyzed using the dynamic eXtended Finite Element Method, and the findings shows excellent agreement with the law of local symmetry ($K_{II} = 0$). The calculated maximum crack speed of about 1250 m/s well agrees with the mirror like fracture surface observed in the experiment.

Acknowledgments

D.S. acknowledges the support of the Israel Science Foundation (ISF) under Grant No. 1110/04. T.B. acknowledges the support of the Office of Naval Research under Grant Nos. N00014-06-1-0380 and N00014-06-1-0266.

References

- [1] Michot G, Badawi K, Abd El Halim AR, George A. X-ray topographic study of crack tip dislocation patterns in silicon. *Philos Mag* 1980;42:195–202.
- [2] Sherman D, Be'ery I. The shape and the energies of a dynamically propagating crack under bending. *J Mater Res* 2003;18:2379–86.
- [3] Ravichandar K, Knauss WG. An experimental investigation into dynamic fracture: I-Crack initiation and arrest. *Int J Fract* 1984;25:247–62.
- [4] Finberg J, Gross SP, Marder M, Swinney HL. Instabilities in dynamic fracture. *Phys Rev Lett* 1991;67:457–60.
- [5] Janssen C. Specimen for fracture mechanics studies on glass. In: Biezeno CB, Burgers JM, editors. *Proceedings of the 10th international congress on glass in Tokyo*; 1974. p. 10.23–10.30.
- [6] Ballarini R, Kahn H, Tayebi N, Heuer AH. Effects of microstructure on the strength and fracture toughness of polysilicon: a wafer level testing approach. *Mech Prop Struct Films ASTM STP* 2001;1413:37–51.
- [7] Cotterell B, Rice JR. Slightly curved or kinked cracks. *Int J Fract* 1980;16:155–69.
- [8] Erdogan F, Sih, GS. A special theory of crack propagation. In: *Mechanics of fracture*, vol. 1, Noordhove, Leiden; 1972.
- [9] Goldstein RV, Salganik RL. Brittle fracture of solids with arbitrary cracks. *Int J Fract* 1974;10:507–27.
- [10] Riddell WT, Ingraffea AR, Wawrzynek PA. Experimental observations and numerical predictions of three-dimensional fatigue crack propagation. *Eng Fract Mech* 1997;58:230–93.
- [11] Bittencourt TN, Wawrzynek PA, Ingraffea AR, Sousa JL. Quasi-automatic simulation of crack propagation for 2D LEFM problems. *Eng Fract Mech* 1996;55:321–34.
- [12] Ortiz M, Pandolfi A. Finite-deformation irreversible cohesive elements for three-dimensional crack-propagation analysis. *Int J Numer Meth Eng* 1999;44:1267–82.
- [13] Wawrzynek P, Ingraffea AR. Interactive finite element analysis of fracture processes: an integrated approach. *Theor Appl Fract Mech* 1987;8:137–50.
- [14] Krysl P, Belytschko T. The element free Galerkin method for dynamic propagation of arbitrary 3-D cracks. *Int J Numer Meth Eng* 1999;44:767–800.
- [15] Moës N, Dolbow J, Belytschko T. A finite element method for crack growth without remeshing. *Int J Numer Meth Eng* 1999;46:131–50.
- [16] Belytschko T, Chen H, Xu J, Zi G. Dynamic crack propagation based on loss of hyperbolicity and a new discontinuous enrichment. *Int J Numer Meth Eng* 2003;58:1873–905.
- [17] Zi G, Belytschko T. New crack-tip elements for XFEM and applications to cohesive cracks. *Int J Numer Meth Eng* 2003;57:2221–40.
- [18] Song JH, Areias PMA, Belytschko T. A method for dynamic crack and shear band propagation with phantom nodes. *Int J Numer Meth Eng* 2006;67:868–93.
- [19] Menouillard T, Réthoré J, Combescure A, Bung H. Efficient explicit time stepping for the eXtended Finite Element Method. *Int J Numer Meth Eng* 2006;68:911–39.
- [20] Belytschko T, Black T. Elastic crack growth in finite elements with minimal remeshing. *Int J Numer Meth Eng* 1999;45:601–20.
- [21] Hansbo A, Hansbo P. A finite element method for the simulation of strong discontinuities in solid mechanics. *Comput Meth Appl Mech Eng* 2004;193:3523–40.
- [22] Belytschko T, Moës N, Usui S, Parimi C. Arbitrary discontinuities in finite elements. *Int J Numer Meth Eng* 2001;50:993–1013.
- [23] Burghard Z, Zimmermann A, Rodel J, Aldinger F, Lawn BR. Crack opening profiles of indentation cracks in normal and anomalous glasses. *Acta Mater* 2004;52:293–7.
- [24] Nishioka T, Stan F. A hybrid experimental-numerical study on the mechanism of three dimensional dynamic fracture. *Comp Model Eng Sci* 2003;4:119–40.
- [25] Tilbrook M, Hoffman M. Implementation of the local symmetry criterion for crack-growth simulations. In: Atrens A, Boland JN, Clegg R, Griffiths JR, editors. *Structural integrity and fracture international conference (SIF'04)*, Brisbane, Australia; 26–29 September 2004. p. 26–29.
- [26] Tilbrook M, Hoffman M. Approximation of curved cracks under mixed-mode loading. *Eng Fract Mech* 2007;74:1026–40.
- [27] Freund LB. Crack propagation in an elastic solid subjected to general loading – I constant rate of extension. *J Mech Phys Solids* 1972;20:129–40.
- [28] Suo XZ, Combescure A. On the application of the $g(\theta)$ method and its comparison with de Lorenzi's approach. *Nucl Eng Des* 1992;135:207–24.
- [29] Menouillard T, Elguedj T, Combescure V. Mixed-mode stress intensity factors for graded materials. *Int J Solids Struct* 2006;43:1946–59.
- [30] Menouillard T, Belytschko T. Analysis and computations of oscillating crack propagation in a heated strip. *Int J Fract* 2011;167:57–70.
- [31] Gross SP, Fineberg J, Marder M, McCormick W, Swinney HL. Acoustic emissions from rapidly moving cracks. *Phys Rev Lett* 1993;71:3162–5.